

Zero-Shot Trajectory Planning for Signal Temporal Logic Tasks

Ruijia Liu¹, Ancheng Hou¹, Xiao Yu², Xiang Yin¹

¹Department of Automation, Shanghai Jiao Tong University

²Institute of Artificial Intelligence, Xiamen University

{liuruijia,hou.ancheng}@sjtu.edu.cn, xiaoyu@xmu.edu.cn, yinxiang@sjtu.edu.cn

Abstract

Signal Temporal Logic (STL) is a powerful specification language for describing complex temporal behaviors of continuous signals, making it well-suited for high-level robotic task descriptions. However, generating executable plans for STL tasks is challenging, as it requires consideration of the coupling between the task specification and the system dynamics. Existing approaches either follow a model-based setting that explicitly requires knowledge of the system dynamics or adopt a task-oriented data-driven approach to learn plans for specific tasks. In this work, we investigate the problem of generating executable STL plans for systems whose dynamics are unknown a priori. We propose a new planning framework that uses only task-agnostic data during the offline training stage, enabling zero-shot generalization to new STL tasks. Our framework is hierarchical, involving: (i) decomposing the STL task into a set of progress and time constraints, (ii) searching for time-aware waypoints guided by task-agnostic data, and (iii) generating trajectories using a pre-trained safe diffusion model. Simulation results demonstrate the effectiveness of our method indeed in achieving zero-shot generalization to various STL tasks.

1 Introduction

Signal Temporal Logic (STL) is a formal specification language used to describe the temporal behavior of continuous signals. It has become widely adopted for specifying high-level robotic behaviors due to its expressiveness and the availability of both Boolean and quantitative evaluation measures. Controlling robots under STL task constraints, however, is a challenging problem, as it requires balancing both the satisfaction of the task and the feasibility of the system dynamics. In cases where the environment and system dynamics are fully known, several representative methods have been developed, including optimization-based approaches [Raman *et al.*, 2014; Kurtz and Lin, 2022; Sun *et al.*, 2022], gradient-based techniques [Gilpin *et al.*, 2020; Dawson and Fan, 2022], and sampling-based methods [Ilyes *et al.*, 2023]. However, these methods are often difficult to

apply in practical scenarios, where the system dynamics and environment are either unknown or difficult to model.

To address the challenge of unknown dynamics, several learning-based approaches have been proposed. One typical method is reinforcement learning (RL) [Aksaray *et al.*, 2016; Balakrishnan and Deshmukh, 2019; Kalagarla *et al.*, 2021; Venkataraman *et al.*, 2020; Ikemoto and Ushio, 2022; Wang *et al.*, 2024], where an appropriate reward function is designed to approximate the satisfaction of the STL task. However, these methods often struggle with long-horizon STL tasks and lack generalization capabilities across different tasks. Another approach involves first learning a system model and then integrating it with model-based planning methods. For example, in [Kapoor *et al.*, 2020], the authors trained a neural network to approximate the system dynamics and combined it with an optimization-based approach. However, this method is limited to simple short-horizon STL tasks due to its high computational cost. In [He *et al.*, 2024], the authors used goal-conditioned RL to train multiple goal-conditioned policies, referred to as “skills,” to accomplish specific objectives. They then applied a search algorithm to determine the optimal sequence of “skills” needed to satisfy the given STL tasks. While this approach enables a certain degree of task generalizations, these tasks must be based on pre-defined objectives associated with the skills.

More recently, generative models, such as diffusion models [Ho *et al.*, 2020], have emerged as a new approach for generating trajectories for systems with unknown dynamics [Janner *et al.*, 2022; Ajay *et al.*, 2022; Chi *et al.*, 2023; Carvalho *et al.*, 2023; Huang *et al.*, 2025], gaining popularity across various applications. Compared to traditional model-based reinforcement learning methods, these generative approaches are better suited for long-horizon decision-making and offer greater test-time flexibility [Janner *et al.*, 2022], making them particularly effective for complex tasks. For example, for finite Linear Temporal Logic (LTL_f) tasks, [Feng *et al.*, 2024a] introduced a classifier-based guidance approach to steer the sampling of diffusion models, ensuring that generated trajectories satisfy LTL_f requirements. Similarly, [Feng *et al.*, 2024b] proposed a hierarchical framework that decomposes co-safe LTL tasks into sub-tasks using hierarchical reinforcement learning. This framework employs a diffusion model with a determinant-based sampling strategy to generate diverse low-level trajectories, improving both

planning success rates and task generalization.

In the context of STL trajectory planning, the use of generative models has also been explored recently. For example, [Zhong *et al.*, 2023] proposed a classifier-based guidance approach that leverages robustness gradients to guide diffusion model sampling, enabling the generation of vehicle trajectories that adhere to traffic rules specified by STL. Building on this, [Meng and Fan, 2024] introduced a data augmentation method to enhance trajectory diversity and improve rule satisfaction rates. However, these approaches are still limited to simpler STL tasks, primarily due to the complexity of optimizing robustness values and the inherent trade-off between maximizing reward objectives and maintaining the feasibility of the generated trajectories [Li *et al.*, 2024].

In this paper, we address the challenge of generating trajectories for complex, long-horizon STL tasks that are feasible for an underlying system with unknown dynamics. Specifically, we assume access only to a set of task-agnostic trajectory data from previous operations. Inspired by recent advances in decomposition-based STL planning [Kapoor *et al.*, 2024], we propose a novel hierarchical framework that integrates task decomposition, search algorithms, and generative models. First, complex STL tasks are decomposed into a set of time-aware reach-avoid progresses and time constraints. Next, a search algorithm, heuristically guided by the trajectory data, is employed to allocate these progresses and generate a sequence of waypoints with corresponding timestamps. Finally, a pre-trained diffusion model, trained on task-agnostic data, is used to sequentially generate trajectories that achieve the timed waypoints, resulting in a complete solution. To the best of our knowledge, our algorithm is the first data-driven approach with zero-shot generalization capabilities for complex STL tasks. Simulation experiments demonstrate that our method achieves a high success rate in trajectory planning across diverse, long-horizon STL tasks and outperforms commonly used non-data-driven methods in terms of efficiency.

2 Preliminaries

2.1 System Model

We consider a discrete time system with unknown dynamics

$$\mathbf{x}_{t+1} = f(\mathbf{x}_t, \mathbf{a}_t), \quad (1)$$

where $\mathbf{x}_t \in \mathbb{R}^n$ and $\mathbf{a}_t \in \mathbb{R}^m$ are the state and the action at time instant t , respectively. Given an initial state \mathbf{x}_0 and a sequence of actions $\mathbf{a}_0 \mathbf{a}_1 \dots \mathbf{a}_{T-1}$, the resulting *trajectory* of the system is $\tau = \mathbf{x}_0 \mathbf{a}_0 \mathbf{x}_1 \mathbf{a}_1 \dots \mathbf{a}_{T-1} \mathbf{x}_T$, where T is the horizon. The *signal* of the trajectory is referred to as the state sequence $\mathbf{s} = \mathbf{x}_0 \mathbf{x}_1 \dots \mathbf{x}_T$ and we denote by $\mathbf{s}_t = \mathbf{x}_t \mathbf{x}_{t+1} \dots \mathbf{x}_T$ the sub-signal starting from time step t .

2.2 Signal Temporal Logic

We use signal temporal logic (STL) to describe the formal task imposed on the generated state sequence [Maler and Nickovic, 2004]. Specifically, we consider STL formula in the Positive Normal Form (PNF) [Sadraddini and Belta, 2015] whose syntax is as follows:

$$\varphi ::= \top \mid \mu \mid \varphi_1 \wedge \varphi_2 \mid \varphi_1 \vee \varphi_2 \mid F_{[a,b]} \varphi \mid G_{[a,b]} \varphi \mid \varphi_1 U_{[a,b]} \varphi_2, \quad (2)$$

where \top is the true predicate and μ is an atomic predicate associated with an evaluation function $h_\mu : \mathbb{R}^n \rightarrow \mathbb{R}$, i.e., predicate μ is true at state \mathbf{x}_t iff $h_\mu(\mathbf{x}_t) \geq 0$. Furthermore, \wedge and \vee are logic operators “conjunction” and “disjunction”, respectively; $U_{[a,b]}$, $F_{[a,b]}$ and $G_{[a,b]}$ are temporal operators “until”, “eventually” and “always”, respectively; $[a, b]$ is a time interval such that $a, b \in \mathbb{Z}, 0 \leq a \leq b < \infty$. Note that, negation is not used in the PNF. However, as shown in [Sadraddini and Belta, 2015], this does not result in any loss of generality as one can always redefine atomic predicates to account for the presence of negations, allowing any general STL formula to be expressed in PNF. In our work, we impose an additional restriction on the Prenex Normal Form of formulas. Specifically, for any formula of the form $\varphi_1 U_{[a,b]} \varphi_2$, φ_1 can only involve temporal operator “always”. This restriction is introduced for technical reasons, as it facilitates the decomposition of the overall formula into a set of progresses.

For any signal $\mathbf{s} = \mathbf{x}_0 \mathbf{x}_1 \dots \mathbf{x}_T$, we denote by $\mathbf{s}_t \models \varphi$ if \mathbf{s} satisfies STL formula φ at time t , and we denote by $\mathbf{s} \models \varphi$ if $\mathbf{s}_0 \models \varphi$. This is formally defined by the Boolean semantics of STL formulae as follows [Bartocci *et al.*, 2018]:

$$\mathbf{s}_t \models \mu \Leftrightarrow h_\mu(\mathbf{x}_t) \geq 0, \quad (3)$$

$$\mathbf{s}_t \models \varphi_1 \wedge \varphi_2 \Leftrightarrow \mathbf{s}_t \models \varphi_1 \wedge \mathbf{s}_t \models \varphi_2, \quad (4)$$

$$\mathbf{s}_t \models \varphi_1 \vee \varphi_2 \Leftrightarrow \mathbf{s}_t \models \varphi_1 \vee \mathbf{s}_t \models \varphi_2, \quad (5)$$

$$\mathbf{s}_t \models F_{[a,b]} \varphi \Leftrightarrow \exists t' \in [t+a, t+b] \text{ s.t. } \mathbf{s}_{t'} \models \varphi, \quad (6)$$

$$\mathbf{s}_t \models G_{[a,b]} \varphi \Leftrightarrow \forall t' \in [t+a, t+b] \text{ s.t. } \mathbf{s}_{t'} \models \varphi, \quad (7)$$

$$\mathbf{s}_t \models \varphi_1 U_{[a,b]} \varphi_2 \Leftrightarrow \exists t' \in [t+a, t+b] \text{ s.t. } \mathbf{s}_{t'} \models \varphi_2 \wedge \forall t'' \in [t, t'], \mathbf{s}_{t''} \models \varphi_1. \quad (8)$$

2.3 Planning with Unknown Dynamics

In the context of STL planning, the objective is to determine an action sequence such that the resulting signal satisfies the specified STL formula. When the system dynamics are perfectly known, this problem can be solved using model-based optimization approaches (e.g., see [Raman *et al.*, 2014; Kurtz and Lin, 2022; Sun *et al.*, 2022]). In contrast, our work addresses a setting with unknown dynamics. Specifically, we assume the mapping $f : \mathbb{R}^n \times \mathbb{R}^m \rightarrow \mathbb{R}^n$ is unknown, but a dataset of historical operational trajectories, consistent with the underlying unknown system dynamics, is available. Note that each trajectory in the dataset is collected from the previous task-agnostic operations and may vary in length. Our goal is to leverage these task-agnostic trajectories to generate new trajectories that satisfy any given STL formula, thereby achieving zero-shot task generalization at test time.

Problem 1. *Given a set of trajectories from the unknown system (1) and a STL formula φ , find a sequence of actions $\mathbf{a}_0 \mathbf{a}_1 \dots \mathbf{a}_T$ such that the resulting signal \mathbf{s} satisfies the STL formula, i.e., $\mathbf{s} \models \varphi$.*

3 Our Method

3.1 Overall Framework

First, we provide an overview of our proposed planning methods, whose overall structure is illustrated in Figure 1. Specifically, our method consists of the following three parts:

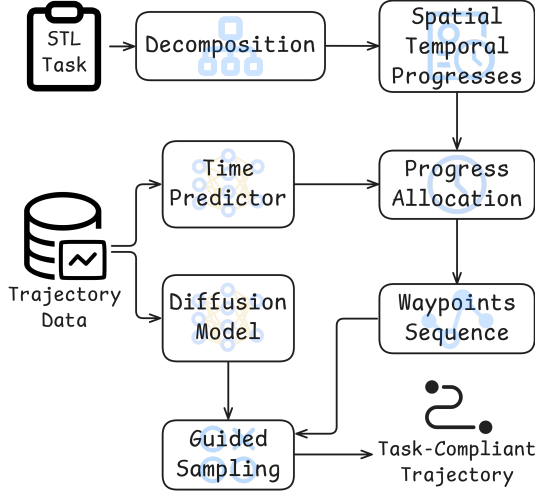


Figure 1: The Overall Framework of Our Proposed Method

- **Task Decomposition:** First, we decompose the given STL into a set of spatial-temporal relevant *progresses* $\mathbb{P} = \mathbb{P}^{\mathcal{R}} \cup \mathbb{P}^{\mathcal{I}}$, where $\mathbb{P}^{\mathcal{R}}$ is the set of *reachability progresses* and $\mathbb{P}^{\mathcal{I}}$ is the set of *invariance progresses*. Furthermore, these progresses need to be satisfied subject to a set of *time constraints* \mathbb{T} over a set of *time variables* Λ .
- **Progress Allocation:** While the decomposition above is task-focused, achieving progress in the correct order requires consideration of the underlying dynamics of the system. To address this, we employ a pre-trained *time predictor* derived from trajectory data to estimate the time required for the system to transition from one waypoint to another. A search-based algorithm is then used to determine a sequence of waypoints with associated timestamps $(\mathbf{x}_0, t_0)(\mathbf{x}_1, t_1) \dots (\mathbf{x}_n, t_n)$ such that each waypoint satisfies the corresponding reachability progress in $\mathbb{P}^{\mathcal{R}}$, and all timestamps comply with the time constraints \mathbb{T} .
- **Trajectory Generation:** The final step is to generate an executable trajectory for the system, ensuring that each waypoint is visited at the correct time while maintaining satisfaction of the invariance progresses. This problem can be framed as several reach-avoid control problems with unknown system dynamics. Our approach leverages a *diffusion model*, pre-trained on trajectory data, to generate task-compliant and dynamic-feasible trajectories through constraints-guided sampling. Following [Ajay *et al.*, 2022], we utilize the diffusion model solely for generating the trajectory’s state sequence. The action sequence can be obtained offline using an inverse dynamics model [Agrawal *et al.*, 2016] or online via appropriate controllers.

Next, we provide the technical details of each part.

3.2 Decompositions of STL Formulae

Eliminating Disjunctions For the given STL task φ , our first step is to convert it into the disjunctive normal form (DNF) $\tilde{\varphi} = \varphi_1 \vee \varphi_2 \vee \dots \vee \varphi_n$, where each subformula φ_i involves no “disjunction”. Formally, for any STL formula, one can obtain its DNF by recursively applying the following replacements:

- replace $F_{[a,b]}(\varphi_1 \vee \varphi_2)$ by $F_{[a,b]}\varphi_1 \vee F_{[a,b]}\varphi_2$;
- replace $G_{[a,b]}(\varphi_1 \vee \varphi_2)$ by $G_{[a,b]}\varphi_1 \vee G_{[a,b]}\varphi_2$;
- replace $(\phi_1 \vee \phi_2)U_{[a,b]}(\varphi_1 \vee \varphi_2)$ by $\bigvee_{i,j \in \{1,2\}} \phi_i U_{[a,b]}\varphi_j$.

Note that the last two replacements are not equivalent, making the resulting DNF $\tilde{\varphi}$ stronger than the original formula φ . Furthermore, to achieve the task defined by $\tilde{\varphi}$, it suffices to satisfy one of the subformulas φ_i . Without loss of generality, we will assume henceforth that the DNF contains only a single subformula, as the STL planning problem can be addressed for each subformula individually. In other words, moving forward, we will focus on STL formulae, denoted directly by φ , without negations (due to the PNF) and without disjunctions (due to the DNF).

Progresses and Constraints Next, we further decompose the overall STL task φ into a set of *progresses*. Specifically, we consider the following two types of progresses:

- **Reachability Progress:** we denote by $\mathcal{R}(a_\Lambda, b_\Lambda, \mu)$ that $\exists t \in [a_\Lambda, b_\Lambda], \mathbf{x}_t \models \mu$.
- **Invariance Progress:** we denoted by $\mathcal{I}(a_\Lambda, b_\Lambda, \mu)$ that $\forall t \in [a_\Lambda, b_\Lambda], \mathbf{x}_t \models \mu$.

Note that we use subscript Λ in time interval $[a_\Lambda, b_\Lambda]$ as a_Λ and b_Λ may not be a fixed time and involve variables in Λ subject to **time constraints**. Therefore, the STL formula φ is decomposed into a tuple $(\mathbb{P}_\varphi, \mathbb{T}_\varphi)$, where \mathbb{P}_φ is the set of progresses and \mathbb{T}_φ is the set of time constraints over variable set Λ . Such decomposition is defined recursively as follows:

- If $\varphi = F_{[a,b]}\mu$, then we have $\mathbb{P}_\varphi = \{\mathcal{R}(\lambda_i, \lambda_i, \mu)\}$ and $\mathbb{T}_\varphi = \{\lambda_i \in [a, b]\}$, where λ_i is a new time variable.
- If $\varphi = G_{[a,b]}\mu$, then we have $\mathbb{P}_\varphi = \{\mathcal{I}(a, b, \mu)\}$ and $\mathbb{T}_\varphi = \emptyset$.
- If $\varphi = \mu_1 U_{[a,b]}\mu_2$, then we have $\mathbb{P}_\varphi = \{\mathcal{I}(a, \lambda_i, \mu_1), \mathcal{R}(\lambda_i, \lambda_i, \mu_2)\}$ and $\mathbb{T}_\varphi = \{\lambda_i \in [a, b]\}$, where λ_i is a new time variable.
- If $\varphi' = \varphi_1 \wedge \varphi_2$, then we merge the progresses and time constraints, i.e., $\mathbb{P}_{\varphi'} = \mathbb{P}_{\varphi_1} \cup \mathbb{P}_{\varphi_2}$ and $\mathbb{T}_{\varphi'} = \mathbb{T}_{\varphi_1} \cup \mathbb{T}_{\varphi_2}$.
- If $\varphi' = F_{[a,b]}\varphi$, then we (i) introduce a new time variable λ_i ; (ii) add a new time constraint $\mathbb{T}_{\varphi'} = \mathbb{T}_\varphi \cup \{\lambda_i \in [a, b]\}$; (iii) increase each time indices in each progress by λ_i , i.e., $\mathbb{P}_{\varphi'} = \{\mathcal{P}(c_\Lambda + \lambda_i, d_\Lambda + \lambda_i, \mu) \mid \mathcal{P}(c_\Lambda, d_\Lambda, \mu) \in \mathbb{P}_\varphi\}$.
- If $\varphi' = G_{[a,b]}\varphi$, then (i) the time constraints remain unchanged, i.e., $\mathbb{T}_{\varphi'} = \mathbb{T}_\varphi$; (ii) modify each invariance progress $\mathcal{I}(c_\Lambda, d_\Lambda, \mu) \in \mathbb{P}_\varphi$ to $\mathcal{I}(c_\Lambda + a, d_\Lambda + b, \mu)$ in $\mathbb{P}_{\varphi'}$; (iii) modify each reachability progress $\mathcal{R}(c_\Lambda, d_\Lambda, \mu) \in \mathbb{P}_\varphi$, to $b - a$ progresses $\mathcal{R}(c_\Lambda + k, d_\Lambda + k, \mu)$ in $\mathbb{P}_{\varphi'}$, where $k = a, a + 1, \dots, b$.
- If $\varphi' = \phi U_{[a,b]}\varphi$, then (i) introduce a new time variable λ_i ; and (ii) add a new time constraint, i.e., $\mathbb{T}_{\varphi'} = \mathbb{T}_\varphi \cup \{\lambda_i \in [a, b]\}$; and (iii) increase each time indices in each progress in \mathbb{P}_φ by λ_i and modify each invariance progress $\mathcal{I}(c_\Lambda, d_\Lambda, \mu) \in \mathbb{P}_\phi$ to $\mathcal{I}(c_\Lambda + a, d_\Lambda + \lambda_i, \mu)$, i.e., $\mathbb{P}_{\varphi'} = \{\mathcal{P}(c_\Lambda + \lambda_i, d_\Lambda + \lambda_i, \mu) \mid \mathcal{P}(c_\Lambda, d_\Lambda, \mu) \in \mathbb{P}_\varphi\} \cup \{\mathcal{I}(c_\Lambda + a, d_\Lambda + \lambda_i, \mu) \mid \mathcal{I}(c_\Lambda, d_\Lambda, \mu) \in \mathbb{P}_\phi\}$.

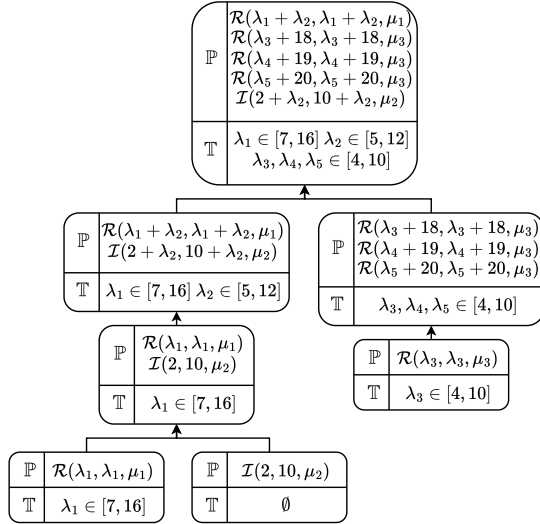


Figure 2: Decomposition Process of STL Formula (9)

To illustrate the above progress decomposition process, we consider the following STL formulae

$$\varphi = F_{[5,12]}(F_{[7,16]}\mu_1 \wedge G_{[2,10]}\mu_2) \wedge G_{[18,20]}F_{[4,10]}\mu_3. \quad (9)$$

The decomposition process is shown in Figure 2, where the progress and time constraints are constructed incrementally from the bottom to the top. The top node represents the overall decomposed $(\mathbb{P}_\varphi, \mathbb{T}_\varphi)$ for the STL formula φ .

3.3 Progress Allocation

Without considering the system dynamics, the STL task planning problem is essentially a constraint satisfaction problem for the decomposed progresses and constraints $(\mathbb{P}_\varphi, \mathbb{T}_\varphi)$. However, the unknown system dynamics introduce additional challenges, as allocating progress arbitrarily may not be feasible for the system. To address this issue, we use a search algorithm to allocate the progresses, where the feasibility of each assignment is determined based on the trajectory data.

To perform the search-based allocation process, we further split the progresses \mathbb{P}_φ as follows. For each invariance progress $\mathcal{I}(a_\Lambda, b_\Lambda, \mu) \in \mathbb{P}_\varphi$, we decompose it into a reachability progress $\mathcal{R}(a_\Lambda, a_\Lambda, \mu)$ and an invariance progress $\mathcal{I}(a_\Lambda + 1, b_\Lambda, \mu)$. For simplicity, we will denote the further decomposed progresses as (\mathbb{P}, \mathbb{T}) without subscripts, where $\mathbb{P} = \mathbb{P}^{\mathcal{R}} \cup \mathbb{P}^{\mathcal{I}}$. Due to this further decomposition, each invariance progress follows a unique reachability progress.

Main Allocation Algorithm The main algorithm for progress allocation is presented in Algorithm 1. The algorithm employs a depth-first search (DFS) to sequentially assign satisfaction times and waypoint for each reachability progress in $\mathbb{P}^{\mathcal{R}}$. When the algorithm terminates, it returns a sequence of waypoints with associated timestamps of form $(x_0, t_0)(x_1, t_1) \dots (x_n, t_n)$ such that each waypoint corresponds to the satisfaction of a reachability progress in $\mathbb{P}^{\mathcal{R}}$. During the search process, we maintain the current state \mathbf{x} , the current time step t , the set of remaining reachability progresses $\mathbb{P}^{\mathcal{R}}$, the set of all time constraints \mathbb{T} , and the searched sequence of waypoints with associated timestamps $\bar{\mathbf{s}}$.

Algorithm 1 Main-Allocation

Require: Initial state \mathbf{x}_0 , start time t_0 , reachability progresses $\mathbb{P}^{\mathcal{R}}$, invariance progresses $\mathbb{P}^{\mathcal{I}}$, time variable constraints \mathbb{T}

Ensure: A valid waypoints sequence $\bar{\mathbf{s}}$ or None if no solution is found

- 1: **Initialize:**
- 2: current state $\mathbf{x} \leftarrow \mathbf{x}_0$; current time $t \leftarrow t_0$
- 3: task sequence $\bar{\mathbf{s}} \leftarrow [(\mathbf{x}, t)]$
- 4: $stack \leftarrow [(\mathbf{x}, t, \mathbb{P}^{\mathcal{R}}, \mathbb{T}, \bar{\mathbf{s}})]$
- 5: **while** $stack$ is not empty **do**
- 6: $(\mathbf{x}, t, \mathbb{P}^{\mathcal{R}}, \mathbb{T}, \bar{\mathbf{s}}) \leftarrow pop(stack)$
- 7: **if** $\mathbb{P}^{\mathcal{R}} = \emptyset$ **then**
- 8: **return** $\bar{\mathbf{s}}, \mathbb{T}$ // All reachability progresses satisfied
- 9: **for each** progress $\mathcal{R}(a_\Lambda, b_\Lambda, \mu) \in \mathbb{P}^{\mathcal{R}}$ **do**
- 10: $t', \mathbf{x}' \leftarrow SampleState(\mathcal{R}(a_\Lambda, b_\Lambda, \mu), \mathbf{x}, t, \mathbb{T}, \mathbb{P}^{\mathcal{I}})$
- 11: **if** $t' \neq None$ **then**
- 12: $\bar{\mathbf{s}}' \leftarrow \bar{\mathbf{s}}.(\mathbf{x}', t')$
- 13: $\mathbb{P}^{\mathcal{R}'} \leftarrow \mathbb{P}^{\mathcal{R}} \setminus \{\mathcal{R}(a_\Lambda, b_\Lambda, \mu)\}$
- 14: $\mathbb{T}' \leftarrow UpdateConstraint(a_\Lambda, b_\Lambda, \mathbb{T}, \mathbf{x}', t')$
- 15: // Push new state onto the stack
- 16: $push(\mathbf{x}', t', \mathbb{P}^{\mathcal{R}'}, \mathbb{T}', \bar{\mathbf{s}}')$ **onto** $stack$
- 17: **end for**
- 18: **end while**
- 19: **return** None // No valid sequence found

At each step, we select a remained reachability progress $\mathcal{R}(a_\Lambda, b_\Lambda, \mu)$ from $\mathbb{P}^{\mathcal{R}}$ as the next target progress from the current state (\mathbf{x}, t) . Specifically, to achieve progress $\mathcal{R}(a_\Lambda, b_\Lambda, \mu)$, function $SampleState$ is used to determine a satisfaction time t' and a corresponding new state \mathbf{x}' such that $\mathbf{x}' \models \mu$. Then the searched waypoint (\mathbf{x}', t') is appended to $\bar{\mathbf{s}}$ and we remove progress $\mathcal{R}(a_\Lambda, b_\Lambda, \mu)$ from $\mathbb{P}^{\mathcal{R}}$. Furthermore, the time constraints \mathbb{T} are updated based on the assigned state \mathbf{x}' and time t' according to function $UpdateConstraint$. Finally, the algorithm proceeds to the next iteration. If $\mathbb{P}^{\mathcal{R}}$ becomes empty, it indicates that all reachability progresses have been successfully assigned a satisfaction time. If no feasible assignment can be made, the algorithm backtracks to explore alternative assignments.

In the above DFS, we use the following heuristic order to select reachability progress from $\mathbb{P}^{\mathcal{R}}$. Let \mathbb{T} be a set of time constraints and a_Λ be an objective function over time variables Λ . We denote by $a_{\Lambda, \mathbb{T}}^{\max}$ and $a_{\Lambda, \mathbb{T}}^{\min}$ the maximum and minimum values of a_Λ under \mathbb{T} , respectively, which can be easily solved by Integer Linear Programming (ILP) techniques. Then during the search process, progress $\mathcal{R}(a_\Lambda, b_\Lambda, \mu)$ with earlier potential deadlines $b_{\Lambda, \mathbb{T}}^{\min}$ are prioritized; and if two progresses have the same deadline, the one with the earlier potential start time $a_{\Lambda, \mathbb{T}}^{\min}$ is preferred.

Constraint Update Let $\mathcal{R}(a_\Lambda, b_\Lambda, \mu)$ be the selected progress and (\mathbf{x}', t') be the assigned waypoint with time. Then we added the following time constraints to \mathbb{T} :

$$a_\Lambda \leq t' \quad \text{and} \quad t' \leq b_\Lambda. \quad (10)$$

Recall that in our decomposition, each original invariance progress $\mathcal{I}(a_\Lambda, b_\Lambda, \mu)$ is decomposed to $\mathcal{R}(a_\Lambda, a_\Lambda, \mu)$ and $\mathcal{I}(a_\Lambda + 1, b_\Lambda, \mu)$. Therefore, if constraints (10) are added for $\mathcal{R}(a_\Lambda, a_\Lambda, \mu)$, it means that the value of a_Λ is determined as t' , and we denoted by $\mathbb{P}_{det}^{\mathcal{I}}$ the set of invariance progresses

Algorithm 2 SampleState

Input: reachability progress $\mathcal{R}(a, b, \mu)$, current state \mathbf{x} , time step t , time variable constraints \mathbb{T} , invariance progresses $\mathbb{P}^{\mathcal{I}}$
Output: Assigned satisfaction time t_{new} of constraint $\mathcal{R}(a, b, \mu)$ and new state \mathbf{x}' or None if no solution is found

- 1: $t_{\min} \leftarrow a_{\Lambda, \mathbb{T}}^{\min}, t_{\max} \leftarrow b_{\Lambda, \mathbb{T}}^{\max}$
- 2: **for** up to N_{\max} attempts **do**
- 3: Sample state \mathbf{x}' such that $\mathbf{x}' \models \mu$
- 4: **Initialize:** conflict time interval $\mathcal{O} \leftarrow \emptyset$
- 5: **for all** $\mathcal{I}(c, d_{\Lambda}, \mu) \in \mathbb{P}_{\text{det}}^{\mathcal{I}}$ with determined starting time **do**
- 6: **if** $\mathbf{x}' \not\models \mu$ **then**
- 7: $\mathcal{O} \leftarrow \mathcal{O} \cup [c, d_{\Lambda, \mathbb{T}}^{\min}]$
- 8: **end if**
- 9: **end for**
- 10: $t' \leftarrow t + \text{TimePredict}(\mathbf{x}, \mathbf{x}')$
- 11: **if** $t' > t_{\max}$ **or** $[\max\{t', t_{\min}\}, t_{\max}] \setminus \mathcal{O} = \emptyset$ **then**
- 12: **Continue** to next sampling attempt
- 13: **end if**
- 14: $t_{\text{new}} \leftarrow$ earliest time in $[\max\{t', t_{\min}\}, t_{\max}] \setminus \mathcal{O}$
- 15: **return** $t_{\text{new}}, \mathbf{x}'$
- 16: **end for**
- 17: **return** None // No valid time found

whose starting times are determined. Then for those invariance progress $\mathcal{I}(c, d_{\Lambda}, \mu) \in \mathbb{P}_{\text{det}}^{\mathcal{I}}$ whose starting time is determined, if $\mathbf{x}' \not\models \mu$, then we further add a new constraint $d_{\Lambda} < t'$, i.e., the invariance progress can only be effective before t' to avoid conflict with the assigned waypoint.

Sample Timed Waypoints When a reachability progress $\mathcal{R}(a_{\Lambda}, b_{\Lambda}, \mu)$ is selected, we use function `SampleState` to determine a valid satisfaction time and waypoint state for this progress while ensuring compliance with invariance progresses. The pseudocode of this function is shown in Algorithm 2. The process starts by computing the largest possible time interval $[t_{\min}, t_{\max}]$ for the reachability progress. Then the algorithm attempts to sample a candidate state \mathbf{x}' with the satisfaction region of μ up to N_{\max} times. For each attempt, we first calculate the minimum possible conflict time interval, denoted by \mathcal{O} , during which \mathbf{x}' conflicts with the invariance progresses. Here, we only consider invariance progresses whose starting times are determined. This is because, in the STL decomposition, each invariance progress follows a “preceding” reachability progress. If the starting time of an invariance progress is not determined, then it implies that its “preceding” reachability progress has not yet been satisfied and will only be satisfied strictly later than the current reachability progress. Consequently, this invariance progress will also start strictly later.

Once the conflict time interval \mathcal{O} is computed, we further use function `TimePredict` to predict the arrival time t' from the current state \mathbf{x} to the sample state \mathbf{x}' . Particularly, if (i) $t' > t_{\max}$; or (ii) the feasible interval $[\max\{t', t_{\min}\}, t_{\max}]$ is fully occupied by conflicting intervals in \mathcal{O} , then it means that the sample state \mathbf{x}' is not feasible and we proceed to the next attempt. Otherwise, the earliest available time t_{new} in the feasible interval is assigned as the satisfaction time, and the algorithm returns t_{new} along with the sampled state \mathbf{x}' .

Prediction of Reachability Time In Algorithm 2, model `TimePredict` is used to estimate the time step (trajectory

length) needed to transition from the current state \mathbf{x} to the new state \mathbf{x}' . This model is trained on the same trajectory data, that will be used to train the Diffusion model. It assumes that the trajectory length between two states follows a Gaussian distribution. A simple multilayer perceptron (MLP) is used as the backbone of `TimePredict` model, and it is trained to predict the mean and variance of the trajectory length using a negative log-likelihood loss function. To account for tasks with avoidance requirements, which may require longer trajectories, a scaling factor γ is applied to the predicted mean trajectory length. This factor allows control over the algorithm’s conservativeness by adjusting the predicted trajectory length as needed.

3.4 Trajectory Generation

In the above part, a sequence of waypoints $\bar{\mathbf{s}}$ is obtained and the time intervals for each invariance progress have also been determined. The remaining task is to generate executable trajectories that connect the waypoints while ensuring the trajectories satisfy the invariance progresses. Specifically, the trajectory τ between two adjacent waypoints (\mathbf{x}_i, t_i) and $(\mathbf{x}_{i+1}, t_{i+1})$ must be feasible under the current system dynamics and satisfy the following conditions:

1. The trajectory length is $t_{i+1} - t_i + 1$.
2. It starts at state \mathbf{x}_i and ends at state \mathbf{x}_{i+1} .
3. It satisfies all invariance progresses active within the time interval $[t_i, t_{i+1}]$.

We employ the diffusion model to solve this conditional trajectory generation problem since it can learn the distribution of system trajectories from system trajectory data, enabling it to generate feasible trajectories under the current system. Additionally, by guiding the sampling process, the generated trajectories can satisfy additional constraints.

The technical details of the diffusion model employed are provided in the **Appendix B**. Here, we briefly outline the main idea. To satisfy the first condition, we control the length of the generated trajectory by adjusting the length of the initial noise during the denoising process. This is feasible due to the structural properties of the backbone network used in the diffusion model [Janner *et al.*, 2022]. For the second condition, we treat it as an inpainting problem [Janner *et al.*, 2022], ensuring that the generated trajectory meets the requirement by replacing the start and end states of the trajectory with \mathbf{x}_i and \mathbf{x}_{i+1} , respectively, after each denoising step. To address the last condition, we decompose each invariance progress $\mathcal{I}(a, b, \mu_i)$ into state constraints of the form $h_{\mu_i}(\mathbf{x}_t) \geq 0$ for $t = a, a + 1, \dots, b$, commonly referred to as “safety” constraints. We employ `SafeDiffuser` [Xiao *et al.*, 2023] to generate trajectories that comply with these safety constraints. `SafeDiffuser` integrates control barrier functions (CBFs) [Nguyen and Sreenath, 2016] to enforce finite-time diffusion invariance directly within the sampling process.

4 Case Study

To illustrate the workflow of our algorithm, we consider a sequential visit and region avoidance task in the Maze2D (Large) environment [Fu *et al.*, 2020].

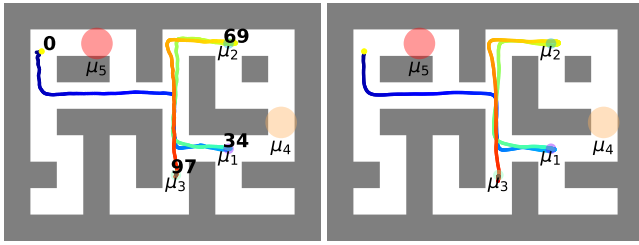


Figure 3: Planned Trajectory (left) and Actual Execution Trajectory (right) in Case Study. The numbers next to start point and regions μ_1 , μ_2 , and μ_3 indicate the completion times for each reachability progress assigned by progress allocation module.

Type	Details
$\mathbb{P}^{\mathcal{R}}$	$\mathcal{R}(\lambda_1, \lambda_1, \mu_1), \mathcal{R}(\lambda_1 + \lambda_2, \lambda_1 + \lambda_2, \mu_2),$ $\mathcal{R}(\lambda_1 + \lambda_2 + \lambda_3, \lambda_1 + \lambda_2 + \lambda_3, \mu_3),$ $\mathcal{R}(0, 0, \neg\mu_4), \mathcal{R}(0, 0, \neg\mu_5)$
$\mathbb{P}^{\mathcal{I}}$	$\mathcal{I}(1, 110, \neg\mu_4), \mathcal{I}(1, 110, \neg\mu_5)$
\mathbb{T}	$\lambda_1 \in [0, 35], \lambda_2 \in [35, 45], \lambda_3 \in [10, 30]$

Table 1: STL Task Decomposition Results

In this scenario, the agent starts at the yellow point shown in Figure 3 and aims to complete the following STL task:

$$F_{[0,35]}(\mu_1 \wedge (F_{[35,45]}(\mu_2 \wedge F_{[10,30]}\mu_3))) \wedge G_{[0,110]}(\neg\mu_4 \wedge \neg\mu_5),$$

where the predicate μ_i represents “reach region μ_i ,” and $\neg\mu_i$ denotes “avoid region μ_i .” Intuitively, this STL task requires the agent to sequentially visit circular regions μ_1 , μ_2 , and μ_3 within specific time intervals while avoiding regions μ_4 and μ_5 throughout the entire episode. The environment layout and target regions are depicted in Figure 3. Our method leverages only an STL task-agnostic trajectory dataset to train the diffusion model, without prior knowledge of the map or system dynamics.

The decomposed progresses and time constraints are summarized in Table 1. The planning algorithm then assigns completion times to each reachability progress, as indicated by the numbers next to start point and regions μ_1 , μ_2 , and μ_3 in Figure 3, resulting in a sequence of waypoints with corresponding times. The diffusion model is then used to sequentially generate trajectories between adjacent waypoints while ensuring all invariance progresses are satisfied. The final generated trajectory is shown in the left subfigure of Figure 3.

Finally, to evaluate the feasibility of the planned trajectory, we employ a simple model-free PD controller to track it. The resulting execution trajectory is shown in the right subfigure of Figure 3. Using the open-source library `stlpy` [Kurtz and Lin, 2022], we calculate the robustness values for both the planned and actual execution trajectories as 0.180 and 0.115, respectively. Since both values are positive, the trajectories satisfy the STL task requirements.

5 Experiments

To evaluate the performance of our algorithm, we further conduct experiments in the Maze2D environment. Specifically,

Type	STL Templates
1	$F_{I_1}\mu_1 \wedge G(\neg\mu_2)$
2	$F_{I_1}\mu_1 \wedge F_{I_2}\mu_2$
3	$F_{I_1}\mu_1 \wedge (\neg\mu_1 U_{I_1}\mu_2)$
4	$F_{I_1}(\mu_1 \wedge (F_{I_2}(\mu_2 \wedge F_{I_3}(\mu_3 \wedge F_{I_4}(\mu_4))))$
5	$F_{I_1}(\mu_1 \wedge (F_{I_2}(\mu_2 \wedge F_{I_3}(\mu_3)))) \wedge G(\neg\mu_4)$
6	$F_{I_1}(\mu_1) \wedge F_{I_2}(\mu_2) \wedge F_{I_3}(\mu_3) \wedge G(\neg\mu_4)$
7	$F_{I_1}(G_{I_2}(\mu_1)) \wedge F_{I_3}(\mu_2) \wedge G(\neg\mu_3)$
8	$F_{I_1}(\mu_1 \wedge F_{I_2}(G_{I_3}(\mu_2)))$
9	$F_{I_1}(\mu_1 \wedge F_{I_2}(\mu_2) \wedge F_{I_3}(\mu_3) \wedge G_{I_4}(\mu_4))$

Table 2: STL Task Templates for Experiments

to validate the zero-shot generalization capability of our algorithm for STL tasks, we test it on a set of testing cases containing randomly generated STL tasks in three different Maze2D environments: U-Maze, Medium, Large. The experimental setup follows the same framework described in the Case Study. The agent starts from a randomly generated position and must complete the randomly generated STL tasks by reaching the target region within the specified time interval. All experiments were conducted on a PC running Ubuntu 22.04, equipped with an Intel i7-13700K CPU and an Nvidia 4090 GPU.

STL Tasks Generation In order to generate random STL tasks, we design nine STL task templates as shown in Table 2. For each template, we randomly generated time intervals and the positions and sizes of circular regions corresponding to atomic predicates in the template, resulting in randomized STL tasks. Specifically, for each pair of Maze2D environment (U-Maze, Medium, Large) and each task template listed in Table 2, we generate 150 feasible random STL formulae.

Baseline Algorithm We compare our algorithm with the method proposed in [Zhong *et al.*, 2023], which adopts classifier-based guidance and directly leverages the gradient of the trajectory’s robustness value to guide the sampling process of the diffusion model, thereby optimizing the robustness of the generated trajectory. The gradient of robustness is calculated by the STLCG method proposed in [Leung *et al.*, 2023]. In the following text, we refer to this algorithm as the Robustness Guided Diffuser (RGD).

Experiment Settings The diffusion models used in both RGD and our algorithm are trained following the procedure in [Janner *et al.*, 2022] using the D4RL dataset [Fu *et al.*, 2020]. A simple multilayer perceptron (MLP) with four fully connected layers is used as the `TimePredict` model in our algorithm and it is also trained using the D4RL dataset. In our experiments, we employ diffusion model to generate only the state sequence of the trajectory and use a simple PD controller to follow the state sequence during running to get the actual execution trajectory.

Evaluation Metrics For each environment and each STL task template, we test RGD and our algorithm on all randomly generated test cases and record the average of the following metrics across all cases:

- **Execution Success Rate (SR):** The proportion of cases where the actual execution trajectory achieve non-negative robustness values.

Env	Type	Success Rate(%) \uparrow		Total Planning Time(s) \downarrow		T1(s)
		RGD	ours	RGD	ours	
U	1	80.00	97.33	13.43 \pm 1.51	0.86 \pm 0.13	0.86
	2	36.67	92.00	16.65 \pm 2.06	0.64 \pm 0.17	0.64
	3	32.00	91.33	19.68 \pm 11.76	1.31 \pm 0.15	1.21
	4	-	90.00	-	1.64 \pm 0.20	1.38
	5	-	84.67	-	2.59 \pm 0.45	2.46
	6	-	86.67	-	2.35 \pm 0.42	2.35
	7	-	89.33	-	1.86 \pm 0.33	1.86
	8	-	97.33	-	0.98 \pm 0.15	0.81
	9	-	88.67	-	1.53 \pm 0.27	1.52
M	1	70.00	94.67	53.90 \pm 5.78	3.74 \pm 0.34	3.74
	2	34.67	89.33	70.69 \pm 8.27	2.72 \pm 0.67	2.72
	3	35.33	83.33	129.87 \pm 27.25	5.53 \pm 0.33	5.43
	4	-	83.33	-	7.09 \pm 0.54	6.80
	5	-	82.00	-	11.36 \pm 1.32	11.22
	6	-	84.67	-	11.76 \pm 1.36	11.76
	7	-	90.00	-	8.01 \pm 1.21	8.00
	8	-	91.33	-	3.87 \pm 0.38	3.71
	9	-	82.67	-	6.53 \pm 0.74	6.52
L	1	34.67	92.00	55.48 \pm 5.31	3.62 \pm 0.33	3.62
	2	16.67	81.33	68.70 \pm 7.65	2.88 \pm 0.63	2.87
	3	26.67	79.33	136.35 \pm 38.12	5.59 \pm 0.34	5.49
	4	-	69.33	-	7.46 \pm 0.52	7.13
	5	-	79.33	-	12.62 \pm 0.75	12.45
	6	-	73.33	-	12.37 \pm 1.35	12.37
	7	-	84.00	-	8.18 \pm 0.68	8.18
	8	-	85.33	-	3.93 \pm 0.33	3.75
	9	-	76.67	-	6.93 \pm 0.60	6.92

Table 3: Result of Experiment in Maze2D Environment. U:U-Maze; M:Medium; L:Large; RGD: Robustness Guided Diffuser; T1:Trajectory Generation Time.

- **Total Planning Time (T0):** The average total running time (in seconds) to plan a trajectory per case.

In addition, we also record the average **Trajectory Generation Time (T1)**, which is the average time spent by the Trajectory Generation module of our algorithm per case. By recording this metric, we analyze the proportion of runtime contributed by each module in our algorithm.

Results and Analysis The experimental results are shown in Table 3. During testing, we found that the Robustness Guided Diffuser works only for simple STL tasks (Types 1 to 3). For more complex tasks, it faces two key issues: **(1) Optimization Challenges:** It is often infeasible to achieve a non-negative robustness value within a limited number of denoising steps; and **(2) High Computational Cost:** Complex tasks require longer trajectory generations and more complex robustness value computations, significantly increasing the computational overhead. As a result, the Robustness Guided Diffuser is suitable only for simple, short-horizon STL tasks.

In contrast, our method decomposes complex STL tasks into several short-horizon trajectory generation tasks under simpler constraints, significantly improving both planning success rate and efficiency. In relatively simple environments such as U-Maze and Medium, our algorithm achieves an actual execution **success rate** of over **80%** across all types of STL tasks. Even in the more complex environment, Large, our algorithm maintains a **success rate** of at least **69%** for all task templates. Additionally, the **total planning time** of

our method is significantly lower than that of the Robustness Guided Diffuser (**more than 10 \times faster**).

By comparing the **Trajectory Generation Time (T1)** and **Total Planning Time (T0)**, we identify trajectory generation as the primary efficiency bottleneck of our algorithm. For tasks with more predicates (Type 4, 9) or those involving “avoid” predicates (Type 3, 5, 6 and 7), runtime increases accordingly. This is mainly because tasks involving more predicates require longer waypoint sequences to satisfy, necessitating multiple calls to the diffusion model for trajectory generation. Additionally, for tasks involving “avoid” predicates, the use of SafeDiffuser requires solving more complex quadratic programming (QP) problems to ensure the trajectories satisfy the invariance progresses, thereby increasing the runtime. Recent advancements in accelerating the sampling process of Diffusion Models [Song *et al.*, 2020; Xiao *et al.*, 2021; Zhou *et al.*, 2025] could further enhance the efficiency of our approach, which will be studied in our future work.

Further Experiments In the above experiments, since the system model in the simulation environment is unknown, we cannot rely on model-based approaches to precisely determine the feasibility of the random generated tasks. Instead, the feasibility of the STL formulas is assessed using our progress allocation module without considering the trajectory generation module. This approach may, to some extent, lead to an optimistic estimation of the success rate of our algorithm. To further evaluate the planning success rate, we utilize a custom-built environment where we have full access to both the environment information and system dynamics. In this setup, we use an optimization-based algorithm as a sound and complete solution [Gilpin *et al.*, 2020] to accurately determine the feasibility of the STL formulas. Experimental results demonstrate that the progress allocation module in our algorithm achieves a success rate of over **80%** across various task scenarios, underscoring its strong completeness and robustness. Details of these additional experiments are provided in the **Appendix C**.

6 Conclusion

This paper introduced a hierarchical framework for trajectory planning under Signal Temporal Logic (STL) constraints. By integrating task decomposition with a diffusion model pre-trained on task-agnostic data, the proposed approach achieved high success rates, scalability, and zero-shot generalization to various STL tasks, while significantly reducing computational costs comparing to baseline algorithm. In future work, we aim to further optimize the progress allocation module by introducing uncertainty-aware time prediction and iterative optimization mechanism. These enhancements are expected to reduce the conservativeness of the algorithm and improve the solution quality. Additionally, we plan to integrate receding horizon control and accelerated diffusion sampling to further enhance the execution success rate and improve the algorithm’s efficiency.

References

- [Agrawal *et al.*, 2016] Pulkit Agrawal, Ashvin V Nair, Pieter Abbeel, Jitendra Malik, and Sergey Levine. Learning to poke by poking: Experiential learning of intuitive physics. *Advances in neural information processing systems*, 29, 2016.
- [Ajay *et al.*, 2022] Anurag Ajay, Yilun Du, Abhi Gupta, Joshua Tenenbaum, Tommi Jaakkola, and Pulkit Agrawal. Is conditional generative modeling all you need for decision-making? *arXiv preprint arXiv:2211.15657*, 2022.
- [Aksaray *et al.*, 2016] Derya Aksaray, Austin Jones, Zhao-dan Kong, Mac Schwager, and Calin Belta. Q-learning for robust satisfaction of signal temporal logic specifications. In *2016 IEEE 55th Conference on Decision and Control (CDC)*, pages 6565–6570. IEEE, 2016.
- [Balakrishnan and Deshmukh, 2019] Anand Balakrishnan and Jyotirmoy V Deshmukh. Structured reward functions using stl. In *Proceedings of the 22nd ACM International Conference on Hybrid Systems: Computation and Control*, pages 270–271, 2019.
- [Bartocci *et al.*, 2018] Ezio Bartocci, Jyotirmoy Deshmukh, Alexandre Donzé, Georgios Fainekos, Oded Maler, Dejan Ničković, and Sriram Sankaranarayanan. Specification-based monitoring of cyber-physical systems: a survey on theory, tools and applications. *Lectures on Runtime Verification: Introductory and Advanced Topics*, pages 135–175, 2018.
- [Botteghi *et al.*, 2023] Nicolò Botteghi, Federico Califano, Mannes Poel, and Christoph Brune. Trajectory generation, control, and safety with denoising diffusion probabilistic models. *arXiv preprint arXiv:2306.15512*, 2023.
- [Carvalho *et al.*, 2023] Joao Carvalho, An T Le, Mark Baierl, Dorothea Koert, and Jan Peters. Motion planning diffusion: Learning and planning of robot motions with diffusion models. In *2023 IEEE/RSJ International Conference on Intelligent Robots and Systems (IROS)*, pages 1916–1923. IEEE, 2023.
- [Chi *et al.*, 2023] Cheng Chi, Zhenjia Xu, Siyuan Feng, Eric Cousineau, Yilun Du, Benjamin Burchfiel, Russ Tedrake, and Shuran Song. Diffusion policy: Visuomotor policy learning via action diffusion. *The International Journal of Robotics Research*, page 02783649241273668, 2023.
- [Christopher *et al.*, 2024] Jacob K Christopher, Stephen Baek, and Ferdinando Fioretto. Constrained synthesis with projected diffusion models. In *The Thirty-eighth Annual Conference on Neural Information Processing Systems*, 2024.
- [Dawson and Fan, 2022] Charles Dawson and Chuchu Fan. Robust counterexample-guided optimization for planning from differentiable temporal logic. In *2022 IEEE/RSJ International Conference on Intelligent Robots and Systems (IROS)*, pages 7205–7212. IEEE, 2022.
- [Feng *et al.*, 2024a] Zeyu Feng, Hao Luan, Pranav Goyal, and Harold Soh. Ltldog: Satisfying temporally-extended symbolic constraints for safe diffusion-based planning. *arXiv preprint arXiv:2405.04235*, 2024.
- [Feng *et al.*, 2024b] Zeyu Feng, Hao Luan, Kevin Yuchen Ma, and Harold Soh. Diffusion meets options: Hierarchical generative skill composition for temporally-extended tasks. *arXiv preprint arXiv:2410.02389*, 2024.
- [Fu *et al.*, 2020] Justin Fu, Aviral Kumar, Ofir Nachum, George Tucker, and Sergey Levine. D4rl: Datasets for deep data-driven reinforcement learning. *arXiv preprint arXiv:2004.07219*, 2020.
- [Gilpin *et al.*, 2020] Yann Gilpin, Vince Kurtz, and Hai Lin. A smooth robustness measure of signal temporal logic for symbolic control. *IEEE Control Systems Letters*, 5(1):241–246, 2020.
- [He *et al.*, 2024] Yiting He, Peiran Liu, and Yiding Ji. Scalable signal temporal logic guided reinforcement learning via value function space optimization. *arXiv preprint arXiv:2408.01923*, 2024.
- [Ho *et al.*, 2020] Jonathan Ho, Ajay Jain, and Pieter Abbeel. Denoising diffusion probabilistic models. *Advances in neural information processing systems*, 33:6840–6851, 2020.
- [Huang *et al.*, 2025] Renming Huang, Yunqiang Pei, Guoqing Wang, Yangming Zhang, Yang Yang, Peng Wang, and Hengtao Shen. Diffusion models as optimizers for efficient planning in offline rl. In *European Conference on Computer Vision*, pages 1–17. Springer, 2025.
- [Ikemoto and Ushio, 2022] Junya Ikemoto and Toshimitsu Ushio. Deep reinforcement learning under signal temporal logic constraints using lagrangian relaxation. *IEEE Access*, 10:114814–114828, 2022.
- [Ilyes *et al.*, 2023] Roland B Ilyes, Qi Heng Ho, and Morteza Lahijanian. Stochastic robustness interval for motion planning with signal temporal logic. In *2023 IEEE International Conference on Robotics and Automation (ICRA)*, pages 5716–5722. IEEE, 2023.
- [Janner *et al.*, 2022] Michael Janner, Yilun Du, Joshua Tenenbaum, and Sergey Levine. Planning with diffusion for flexible behavior synthesis. In *International Conference on Machine Learning*, pages 9902–9915. PMLR, 2022.
- [Kalagarla *et al.*, 2021] Krishna C Kalagarla, Rahul Jain, and Pierluigi Nuzzo. Model-free reinforcement learning for optimal control of markov decision processes under signal temporal logic specifications. In *2021 60th IEEE Conference on Decision and Control (CDC)*, pages 2252–2257. IEEE, 2021.
- [Kapoor *et al.*, 2020] Parv Kapoor, Anand Balakrishnan, and Jyotirmoy V Deshmukh. Model-based reinforcement learning from signal temporal logic specifications. *arXiv preprint arXiv:2011.04950*, 2020.
- [Kapoor *et al.*, 2024] Parv Kapoor, Eunsuk Kang, and Rômulo Meira-Góes. Safe planning through incremental decomposition of signal temporal logic specifications.

- In *NASA Formal Methods Symposium*, pages 377–396. Springer, 2024.
- [Kurtz and Lin, 2022] Vincent Kurtz and Hai Lin. Mixed-integer programming for signal temporal logic with fewer binary variables. *IEEE Control Systems Letters*, 6:2635–2640, 2022.
- [Leahy *et al.*, 2023] Kevin Leahy, Makai Mann, and Cristian-Ioan Vasile. Rewrite-based decomposition of signal temporal logic specifications. In *NASA Formal Methods Symposium*, pages 224–240. Springer, 2023.
- [Leung *et al.*, 2023] Karen Leung, Nikos Aréchiga, and Marco Pavone. Backpropagation through signal temporal logic specifications: Infusing logical structure into gradient-based methods. *The International Journal of Robotics Research*, 42(6):356–370, 2023.
- [Li *et al.*, 2024] Xiner Li, Yulai Zhao, Chenyu Wang, Gabriele Scalia, Gokcen Eraslan, Surag Nair, Tommaso Biancalani, Shuiwang Ji, Aviv Regev, Sergey Levine, et al. Derivative-free guidance in continuous and discrete diffusion models with soft value-based decoding. *arXiv preprint arXiv:2408.08252*, 2024.
- [Maler and Nickovic, 2004] Oded Maler and Dejan Nickovic. Monitoring temporal properties of continuous signals. In *International Symposium on Formal Techniques in Real-Time and Fault-Tolerant Systems*, pages 152–166. Springer, 2004.
- [Meng and Fan, 2024] Yue Meng and Chuchu Fan. Diverse controllable diffusion policy with signal temporal logic. *IEEE Robotics and Automation Letters*, 2024.
- [Mizuta and Leung,] Kazuki Mizuta and Karen Leung. Cobl-diffusion: Diffusion-based conditional robot planning in dynamic environments using control barrier and lyapunov functions.
- [Nguyen and Sreenath, 2016] Quan Nguyen and Koushil Sreenath. Exponential control barrier functions for enforcing high relative-degree safety-critical constraints. In *2016 American Control Conference (ACC)*, pages 322–328. IEEE, 2016.
- [Raman *et al.*, 2014] Vasumathi Raman, Mehdi Maasoumy, and Alexandre Donzé. Model predictive control from signal temporal logic specifications: A case study. In *Proceedings of the 4th ACM SIGBED International Workshop on Design, Modeling, and Evaluation of Cyber-Physical Systems*, pages 52–55, 2014.
- [Sadraddini and Belta, 2015] Sadra Sadraddini and Calin Belta. Robust temporal logic model predictive control. In *2015 53rd Annual Allerton Conference on Communication, Control, and Computing (Allerton)*, pages 772–779. IEEE, 2015.
- [Song *et al.*, 2020] Jiaming Song, Chenlin Meng, and Stefano Ermon. Denoising diffusion implicit models. *arXiv preprint arXiv:2010.02502*, 2020.
- [Sun *et al.*, 2022] Dawei Sun, Jingkai Chen, Sayan Mitra, and Chuchu Fan. Multi-agent motion planning from signal temporal logic specifications. *IEEE Robotics and Automation Letters*, 7(2):3451–3458, 2022.
- [Venkataraman *et al.*, 2020] Harish Venkataraman, Derya Aksaray, and Peter Seiler. Tractable reinforcement learning of signal temporal logic objectives. In *Learning for Dynamics and Control*, pages 308–317. PMLR, 2020.
- [Wang *et al.*, 2024] Siqi Wang, Shaoyuan Li, Li Yin, and Xiang Yin. Synthesis of temporally-robust policies for signal temporal logic tasks using reinforcement learning. In *2024 IEEE International Conference on Robotics and Automation (ICRA)*, pages 10503–10509. IEEE, 2024.
- [Xiao *et al.*, 2021] Zhisheng Xiao, Karsten Kreis, and Arash Vahdat. Tackling the generative learning trilemma with denoising diffusion gans. *arXiv preprint arXiv:2112.07804*, 2021.
- [Xiao *et al.*, 2023] Wei Xiao, Tsun-Hsuan Wang, Chuang Gan, and Daniela Rus. Safediffuser: Safe planning with diffusion probabilistic models. *arXiv preprint arXiv:2306.00148*, 2023.
- [Yu *et al.*, 2023] Xinyi Yu, Chuwei Wang, Dingran Yuan, Shaoyuan Li, and Xiang Yin. Model predictive control for signal temporal logic specifications with time interval decomposition. In *2023 62nd IEEE Conference on Decision and Control (CDC)*, pages 7849–7855. IEEE, 2023.
- [Zheng *et al.*, 2024] Yanan Zheng, Jianxiong Li, Dongjie Yu, Yujie Yang, Shengbo Eben Li, Xianyuan Zhan, and Jingjie Liu. Safe offline reinforcement learning with feasibility-guided diffusion model. *arXiv preprint arXiv:2401.10700*, 2024.
- [Zhong *et al.*, 2023] Ziyuan Zhong, Davis Remppe, Danfei Xu, Yuxiao Chen, Sushant Veer, Tong Che, Baishakhi Ray, and Marco Pavone. Guided conditional diffusion for controllable traffic simulation. In *2023 IEEE International Conference on Robotics and Automation (ICRA)*, pages 3560–3566. IEEE, 2023.
- [Zhou *et al.*, 2024a] Guangyao Zhou, Sivaramakrishnan Swaminathan, Rajkumar Vasudeva Raju, J Swaroop Guntupalli, Wolfgang Lehrach, Joseph Ortiz, Antoine Dedieu, Miguel Lázaro-Gredilla, and Kevin Murphy. Diffusion model predictive control. *arXiv preprint arXiv:2410.05364*, 2024.
- [Zhou *et al.*, 2024b] Siyuan Zhou, Yilun Du, Shun Zhang, Mengdi Xu, Yikang Shen, Wei Xiao, Dit-Yan Yeung, and Chuang Gan. Adaptive online replanning with diffusion models. *Advances in Neural Information Processing Systems*, 36, 2024.
- [Zhou *et al.*, 2025] Wenyang Zhou, Zhiyang Dou, Zeyu Cao, Zhouyingcheng Liao, Jingbo Wang, Wenjia Wang, Yuan Liu, Taku Komura, Wenping Wang, and Lingjie Liu. Emdm: Efficient motion diffusion model for fast and high-quality motion generation. In *European Conference on Computer Vision*, pages 18–38. Springer, 2025.

A Related Works

A.1 STL Decomposition

To address the high complexity of STL control synthesis problems, several decomposition-based methods have been proposed [Leahy *et al.*, 2023; Yu *et al.*, 2023; Kapoor *et al.*, 2024]. In [Leahy *et al.*, 2023], the authors proposed a formula transformation-based method for multi-agent STL planning. This approach jointly decomposes an STL specification and team of agents. In [Yu *et al.*, 2023], the authors decompose STL tasks into several subtasks with non-overlapping time intervals using time interval decomposition and sequentially apply the shrinking horizon Model Predictive Control (MPC) algorithm to each short-time-interval subtask. However, this method is limited to handling STL fragments that do not include nested temporal logic operators.

The work most similar to our STL decomposition framework is [Kapoor *et al.*, 2024]. This work first decomposes STL tasks into several spatio-temporal subtasks with time variable constraints. Then, through time variable simplification, partial ordering, and slicing, the subtasks are segmented into several time intervals. Finally, a planning algorithm is subsequently used to sequentially solve the atomic tasks within each time interval. Our algorithm similarly begins by decomposing the STL task into several spatio-temporal progresses and time variable constraints. However, we adopt a search-based approach to determine the completion times and corresponding states to achieve each progress. During the search process, our method dynamically maintains the time variable constraints on-the-fly according to the completion of progresses. By incorporating the search mechanism, our algorithm achieves greater completeness compared to the incremental planning approach used in [Kapoor *et al.*, 2024]. Additionally, the dynamic maintenance of time variable constraints enables a more natural handling of relationships between subtasks and extends the applicability of our approach to more complex STL task fragments that allows “until” operator.

A.2 Planning with Diffusion Model

Recent advancements in diffusion-based planning methods highlight their remarkable flexibility, as they rely exclusively on offline trajectory datasets and do not require direct interaction with or access to the environment. By leveraging guided sampling, these methods can address a wide range of objectives without the need for retraining. This approach has been widely applied to long-horizon task planning and decision-making, facilitating the generation of states or actions for control purposes [Janner *et al.*, 2022; Ajay *et al.*, 2022; Chi *et al.*, 2023].

In the domain of diffusion-based planning for temporal logic tasks, several significant studies have been conducted [Zhong *et al.*, 2023; Meng and Fan, 2024; Feng *et al.*, 2024a; Feng *et al.*, 2024b]. For instance, [Feng *et al.*, 2024a] proposed a classifier-based guidance approach to direct the sampling process of the diffusion model, enabling the generation of trajectories that fulfill finite Linear Temporal Logic (LTL_f) tasks. Similarly, [Feng *et al.*, 2024b] introduced a data-driven hierarchical framework that decomposes co-safe LTL tasks

into sub-tasks using hierarchical reinforcement learning. This framework integrates a diffusion model with a determinant-based sampling technique to efficiently produce diverse low-level trajectories, enhancing both planning success rates and task generalization capabilities.

For diffusion-based Signal Temporal Logic (STL) planning, [Zhong *et al.*, 2023] employed a classifier-based guidance method that leverages the gradient of robustness values to guide the sampling process of a diffusion model. This method enabled the generation of vehicle trajectories compliant with STL-specified traffic rules. Expanding on this work, [Meng and Fan, 2024] introduced a data augmentation process to further improve trajectory diversity and increase the satisfaction rate of specified rules. However, these approaches remain constrained to relatively simple STL tasks due to the inherent complexity of optimizing robustness values, as well as the trade-off between maximizing reward objectives and preserving the feasibility of generated trajectories [Li *et al.*, 2024].

We compare our algorithm with the method proposed in [Zhong *et al.*, 2023] in the experiments. The results demonstrate that our algorithm can handle complex and long-horizon STL tasks that the method in [Zhong *et al.*, 2023] cannot address, while also exhibiting significant advantages in runtime efficiency.

B Diffusion Models for Trajectory Planning

The core concept of diffusion-model-based trajectory planning [Janner *et al.*, 2022; Ajay *et al.*, 2022] is to employ the diffusion model to learn the distribution of pre-collected trajectories $q(\tau^0)$ in the current environment under the system dynamics, thereby transforming planning or control synthesis problems into conditional trajectory generation.

Diffusion models consist of two processes: the **diffusion process** and the **denoising process**.

The **diffusion process** gradually adds Gaussian noise to a trajectory τ^0 , transforming it into noise. At each timestep i , the noisy trajectory is given by:

$$q(\tau^i | \tau^{i-1}) = \mathcal{N}(\tau^i; \sqrt{1 - \beta_i} \tau^{i-1}, \beta_i \mathbf{I}), \quad (\text{B.1})$$

where β_i controls the noise scale, and N is the total number of diffusion steps. The noisy trajectory τ^i at any step can be directly computed as:

$$\tau^i = \sqrt{\bar{\alpha}_i} \tau^0 + \sqrt{1 - \bar{\alpha}_i} \varepsilon, \quad \varepsilon \sim \mathcal{N}(\mathbf{0}, \mathbf{I}), \quad (\text{B.2})$$

with $\bar{\alpha}_i = \prod_{j=1}^i (1 - \beta_j)$.

The **denoising process** reverses the diffusion by iteratively recovering the trajectory from Gaussian noise. The reverse distribution is approximated as:

$$p_\theta(\tau^{i-1} | \tau^i) = \mathcal{N}(\tau^{i-1}; \mu_\theta(\tau^i, i), \Sigma^i), \quad (\text{B.3})$$

where $\mu_\theta(\tau^i, i)$ is parameterized by the model, and Σ^i is typically fixed. Instead of learning μ_θ directly, the model typically predicts the noise $\varepsilon_\theta(\tau^i, i)$ and gets $\mu_\theta(\tau^i, i)$ according to the relationship [Ho *et al.*, 2020]:

$$\mu_\theta(\tau^i, i) = \frac{1}{\sqrt{\alpha_i}} \left(\tau^i - \frac{1 - \alpha_i}{\sqrt{1 - \bar{\alpha}_i}} \varepsilon_\theta(\tau^i, i) \right). \quad (\text{B.4})$$

The model is trained by minimizing a simplified loss function:

$$\mathcal{L}(\theta) = \mathbb{E}_{i, \varepsilon, \tau^0} \left[\|\varepsilon - \varepsilon_\theta(\tau^i, i)\|_2^2 \right]. \quad (\text{B.5})$$

In this paper, superscripts denote the diffusion time step, while subscripts indicate the trajectory time step. For example, τ_t^i represents the state at trajectory time step t during diffusion time step i . For noise-free trajectories, τ^0 , we omit the superscript when there is no ambiguity.

B.1 Safe Planning with Diffusion Model

Previous studies [Xiao *et al.*, 2023; Botteghi *et al.*, 2023; Mizuta and Leung, ; Zheng *et al.*, 2024; Christopher *et al.*, 2024] have demonstrated the effectiveness of diffusion models in generating safety constraint-compliant trajectories. In this work, we employ SafeDiffuser [Xiao *et al.*, 2023], which integrates control barrier functions (CBFs) [Nguyen and Sreenath, 2016] to enforce finite-time diffusion invariance directly within the sampling process.

SafeDiffuser models the denoising process as a dynamic system:

$$\dot{\tau}^i = \lim_{\Delta\tau \rightarrow 0} \frac{\tau^i - \tau^{i+1}}{\Delta\tau} = \mathbf{u}^i, \quad (\text{B.6})$$

where $\Delta\tau$ represents the diffusion time step, and \mathbf{u}^i is a control variable with the same dimension as τ^i .

For each constraint $b(\mathbf{x}_t) = h_{\mu_i}(\mathbf{x}_t) \geq 0$, we define the associated CBF constraints as:

$$\frac{db(\mathbf{x}_t^i)}{d\mathbf{x}_t^i} \mathbf{u}_t^i + \alpha(b(\mathbf{x}_t^i)) \geq 0, \quad \forall i \in \{0, \dots, N-1\}, \quad (\text{B.7})$$

where α is an extended class- \mathcal{K} function, and N is the total number of diffusion time steps.

To ensure compliance with these constraints while minimally altering the denoising process, the optimal control \mathbf{u}^{i*} is computed at each diffusion time step i by solving the following quadratic programming (QP) problem:

$$\begin{aligned} & \text{minimize} && \left\| \mathbf{u}^i - \frac{\tau^i - \tau^{i+1}}{\Delta\tau} \right\|^2, \\ & \text{subject to} && \frac{db(\mathbf{x}_t^i)}{d\mathbf{x}_t^i} \mathbf{u}_t^i + \alpha(b(\mathbf{x}_t^i)) \geq 0. \end{aligned} \quad (\text{B.8})$$

The updated state τ^{i*} is then computed by substituting $\mathbf{u}^i = \mathbf{u}^{i*}$ into (B.6), and τ^i is replaced with τ^{i*} . The complete denoising procedure is summarized in Algorithm 3.

B.2 Time-aware Trajectory Planning

As noted in [Janner *et al.*, 2022], the planning horizon of a diffusion model is not fixed by its architecture but dynamically adapts based on the input noise size. This allows for variable-length plans during the denoising process at test time. In this work, we leverage this adaptability by directly adjusting the input noise size to generate trajectories of the desired length.

During experiments, we observe that models trained with longer planning horizons generalize better to different trajectory lengths during testing. In contrast, models trained with shorter planning horizons exhibit weaker generalization. To address this, we recommend either:

Algorithm 3 Safe Planning with Diffusion Model

Input: Trajectory length T , start state \mathbf{x}_s , goal state \mathbf{x}_g , invariance constraints $\{b(\mathbf{x}_t) \geq 0\}$

Output: A trajectory τ of length T that satisfies all constraints

- 1: Initialize $\tau^N \sim \mathcal{N}(\mathbf{0}, \mathbf{I})$ with length T
 - 2: Replace $\mathbf{x}_0, \mathbf{x}_T$ in τ^N with $\mathbf{x}_s, \mathbf{x}_g$
 - 3: **for** $i = N-1, \dots, 0$ **do**
 - 4: $\boldsymbol{\mu}^{i+1} = \frac{1}{\sqrt{\alpha_{i+1}}}(\tau^{i+1} - \frac{1-\alpha_{i+1}}{\sqrt{1-\alpha_{i+1}}}\varepsilon_\theta(\tau^{i+1}, i+1))$
 - 5: $\tau^i \sim \mathcal{N}(\boldsymbol{\mu}^{i+1}, \boldsymbol{\Sigma}^{i+1})$
 - 6: Solve the QP (B.8) and get \mathbf{u}^{i*}
 - 7: Calculate τ^{i*} by setting $\mathbf{u}^i = \mathbf{u}^{i*}$ in (B.6)
 - 8: $\tau^i \leftarrow \tau^{i*}$
 - 9: Replace $\mathbf{x}_0, \mathbf{x}_T$ in τ^i with $\mathbf{x}_s, \mathbf{x}_g$
 - 10: **end for**
 - 11: **return** τ^0
-

- Using variable horizons during training instead of a fixed horizon, or
- Employing multiple models trained with different horizons to generate trajectories of diverse lengths.

C Comparative Experiment with Optimization-based Method

To further evaluate the success rate of the progress allocation module in our algorithm, we compare it against a widely-used optimization-based algorithm [Gilpin *et al.*, 2020] in a custom-built simulation environment. The baseline algorithm is employed as a sound and complete solution to accurately assess the feasibility of randomly generated test cases.

The experiment is conducted within a bounded 10×10 square 2D plane containing a circular obstacle. The underlying system dynamics are modeled using a double integrator. The agent starts from a randomly generated position and must complete the randomly generated STL tasks by reaching the target region within the specified time interval.

In this experiment, the baseline algorithm is implemented using the open-source library `stlpy` [Kurtz and Lin, 2022] and has full knowledge of the environmental information and system dynamics, while our algorithm only has access to the trajectory dataset.

To generate the trajectory dataset, we randomly sample start and end points in the environment and use the baseline algorithm to solve reach-avoid tasks. This process produces 200,000 collision-free trajectories that satisfy the system dynamics, which are then used to train the diffusion model.

Following the training procedure from [Janner *et al.*, 2022], we train two diffusion models with different planning horizons, as described in Section B.2. The first model is trained on trajectory segments of length 16 for short trajectories, while the second model uses segments of length 32 to improve generalization to longer trajectories.

We generate 200 feasible STL tasks for each template, as described in Section 5. The deterministic baseline algorithm is used to ensure the feasibility of these tasks. However, for templates 4 and 5, which involve multi-layer nesting of temporal operators, the baseline algorithm fails to find solutions

Type	SR0(%)	SR(%)	Total Planning Time(s)↓	
			ours	baseline
1	96.0	93.5	0.99±0.08	3.82±1.44
2	98.0	96.5	0.81±0.03	6.30±1.36
3	96.0	89.0	1.26±0.05	31.60±10.46
4	-	78.5	2.10±0.26	Timeout
5	-	83.0	2.57±0.10	Timeout
6	97.5	69.5	2.87±0.12	24.23±6.39
7	80.0	73.5	1.80±0.08	7.71±3.50
8	89.5	89.0	0.82±0.03	106.58±82.19
9	81.0	72.0	1.61±0.06	151.19±78.82

Table C.1: Result of Experiment in Custom-built Environment. SR0: Progress Allocation Success Rate; SR: Execution Success Rate;

within an acceptable time. In these cases, we still employ our algorithm’s progress allocation module to verify feasibility.

In addition to the **Execution Success Rate (SR)** and **Total Planning Time (T0)** metrics described in Section 5, we introduce an additional evaluation metric:

- **Progress Allocation Success Rate (SR0):** The proportion of cases where the progress allocation module successfully identifies a sequence of waypoints. This metric specifically measures the reliability of the progress allocation module in our algorithm.

The experimental results are summarized in Table C.1. Our algorithm achieves consistently high success rates across test cases generated from diverse task templates. Notably, the **Execution Success Rate (SR)** exceeds 70% in all scenarios, demonstrating the algorithm’s strong generalization capability for STL tasks.

For all templates except 4 and 5, the **Progress Allocation Success Rate (SR0)** exceeds **80%**, indicating that the progress allocation module is generally reliable, albeit slightly conservative.

Finally, by comparing the **Total Planning Time**, our algorithm significantly outperforms the optimization-based baseline algorithm, highlighting the efficiency of the task decomposition and planning framework employed in our approach. Notably, for templates 4 and 5, which involve multi-layered nested STL tasks, the baseline algorithm fails to find feasible solutions within a reasonable time. In contrast, our algorithm demonstrates both high success rates and high efficiency, even in these complex scenarios.

D Implementation Details of Experiments

D.1 Trajectory Generation

In this work, we employ diffusion model to generate only the state sequence of the trajectory to avoid the practical issues discussed in [Ajay *et al.*, 2022]. During testing, we use a simple PD controller to follow the state sequence to get the action sequence on-the-fly and generate the final actual execution trajectory, as it performs better than employing an inverse dynamics model used in [Ajay *et al.*, 2022] to generate actions.

D.2 Calculation of the Robustness Value

Besides the Boolean semantics, STL also incorporates a concept of robustness, which refers to its quantitative semantics used to measure the degree to which a signal satisfies or violates a formula. Positive robustness values signify satisfaction, while negative values indicate violation. The quantitative semantics of a STL formula φ with respect to a signal \mathbf{s}_t starting at time t are defined as follows:

$$\begin{aligned}
\rho(\mathbf{s}_t, \top) &= \rho_{\max}, \text{ where } \rho_{\max} > 0, \\
\rho(\mathbf{s}_t, \mu) &= h_{\mu}(\mathbf{x}_t), \\
\rho(\mathbf{s}_t, \neg\mu) &= -h_{\mu}(\mathbf{x}_t), \\
\rho(\mathbf{s}_t, \varphi_1 \wedge \varphi_2) &= \min(\rho(\mathbf{s}_t, \varphi_1), \rho(\mathbf{s}_t, \varphi_2)), \\
\rho(\mathbf{s}_t, \varphi_1 \vee \varphi_2) &= \max(\rho(\mathbf{s}_t, \varphi_1), \rho(\mathbf{s}_t, \varphi_2)), \\
\rho(\mathbf{s}_t, F_{[a,b]}\varphi) &= \max_{t' \in [t+a, t+b]} \rho(\mathbf{s}_{t'}, \varphi), \\
\rho(\mathbf{s}_t, G_{[a,b]}\varphi) &= \min_{t' \in [t+a, t+b]} \rho(\mathbf{s}_{t'}, \varphi), \\
\rho(\mathbf{s}_t, \varphi_1 U_{[a,b]}\varphi_2) &= \max_{t' \in [t+a, t+b]} \min\{\rho(\mathbf{s}_{t'}, \varphi_2), \\
&\quad \min_{\tau \in [t, t']} \rho(\mathbf{s}_{\tau}, \varphi_1)\}.
\end{aligned} \tag{D.1}$$

In the experiments, we utilized the commonly adopted open-source library `stlpy` [Kurtz and Lin, 2022] to compute the robustness values of both the planned trajectories and the actual execution trajectories. In the Maze2D environment, transitions between states require relatively long trajectories, which result in extended time intervals for the corresponding STL tasks. This creates computational overhead for calculating robustness values using `stlpy`, exceeding the capacity of the experimental hardware.

To address this issue, we introduced an additional sampling factor, η , which represents the mapping relationship between the time length in the STL task and the actual system trajectory. Specifically, we assume that each time step in the STL task corresponds to a trajectory length of η in the system. When computing robustness values, we sample one state from the system trajectory for every η states, resulting in a sampled trajectory. The robustness value is then calculated based on this sampled trajectory. While this operation may introduce minor deviations in the robustness value calculations, it does not affect the validity of the experimental conclusions.

D.3 Experimental Parameter Settings

Some of the parameters involved in the experiments are listed below, and their specific values are shown in Table D.1:

- **Maximum Number of Attempts (N_{\max}):** The maximum number of attempts for new state sampling in Algorithm 2.
- **Horizon (H):** The planning horizon used during the training of the diffusion model.
- **Total Denoise Steps (N):** The total number of steps in the denoising process.
- **Scaling Factor (γ):** Applied to the predicted mean trajectory length, used to control the conservativeness of the Progress Allocation Module, as described in Section 3.3.

Env	N_{\max}	H	N	γ	η
Maze2D-Umaze	1	128	64	0.8	8
Maze2D-Medium	1	256	256	0.9	8
Maze2D-Large	1	384	256	1.1	8
Custom-Built Env	1	16&32	64	1	1

Table D.1: Parameters Used in the Experiments

- **Sampling Factor (η)**: Used when computing the robustness value of trajectories, as described in Section D.2.

E More Cases

We visualized some of the experimental results. The actual execution trajectories for some successful cases (where the STL tasks were satisfied by the execution trajectories) are shown in Figure E.1 to Figure E.3. For some failed cases (where the STL tasks were not satisfied), the trajectories planned by our algorithm are shown in Figure E.4.

Notably, by analyzing the failed cases, we identified that the primary reason for execution failure is that the trajectories generated by the diffusion model significantly violated system dynamics, such as colliding with obstacles in the environment or having excessively large distances between consecutive states. To further enhance the actual execution success rate, our method can be integrated with some receding horizon control methods [Zhou *et al.*, 2024a] or online re-planning strategies [Zhou *et al.*, 2024b]. This extension will be explored in our future work.

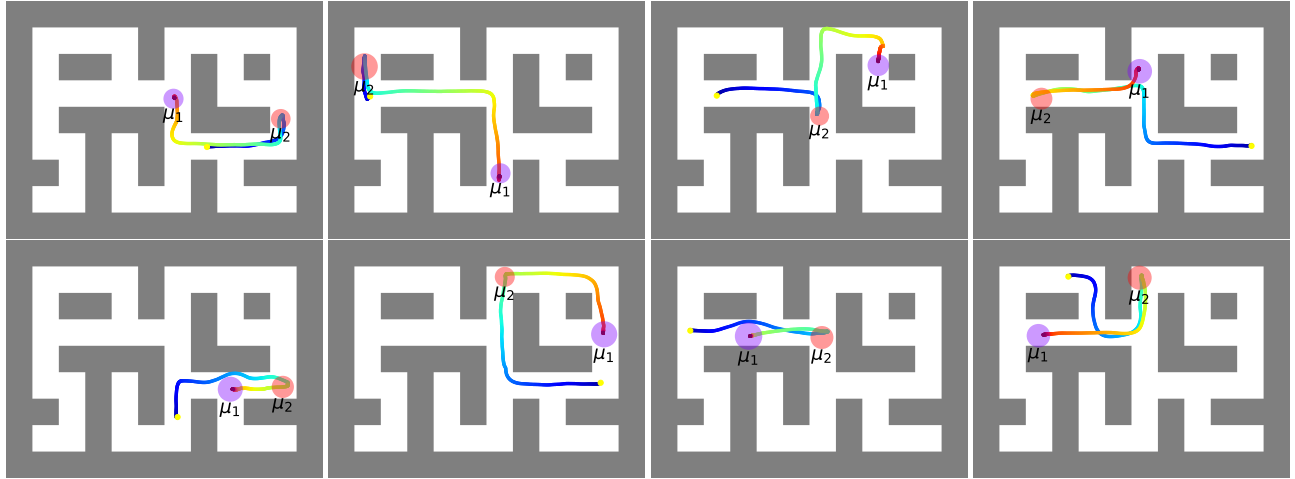


Figure E.1: Successful Execution Trajectories in Maze2D-large Environment under STL Template 3: $F_{I_1} \mu_1 \wedge (\neg \mu_1 \cup_{I_1} \mu_2)$. The task requires the agent to eventually reach region μ_1 within a given time interval, but before reaching μ_1 , it must first visit region μ_2 .

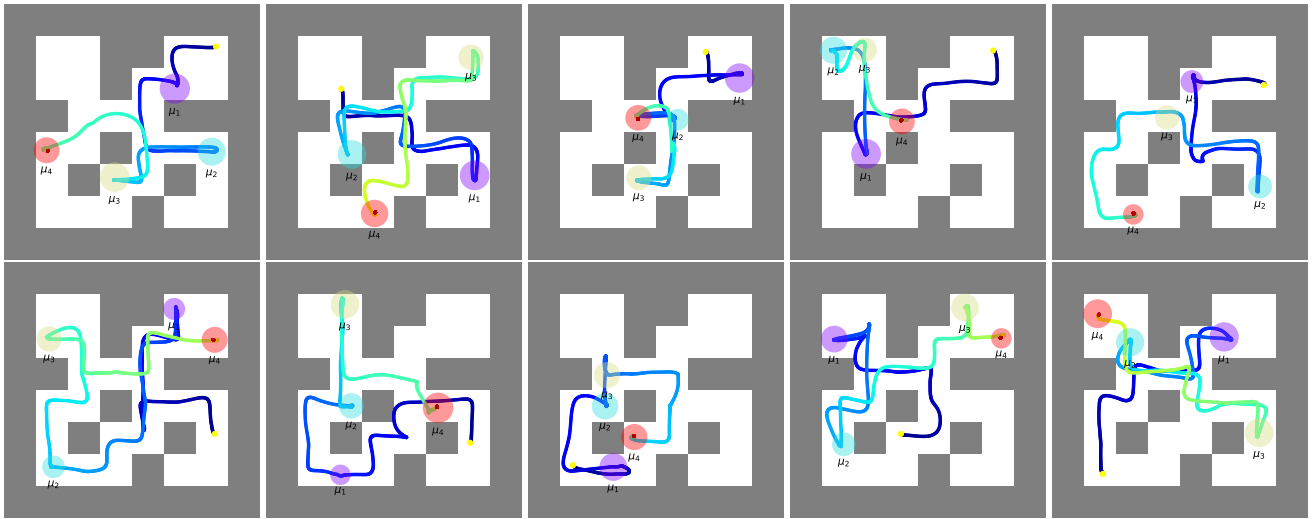


Figure E.2: Successful Execution Trajectories in Maze2D-medium Environment under STL Template 4: $F_{I_1}(\mu_1 \wedge (F_{I_2}(\mu_2 \wedge F_{I_3}(\mu_3 \wedge F_{I_4}(\mu_4))))))$. The task requires the agent to sequentially visit regions $\mu_1, \mu_2, \mu_3, \mu_4$ within the given time intervals.

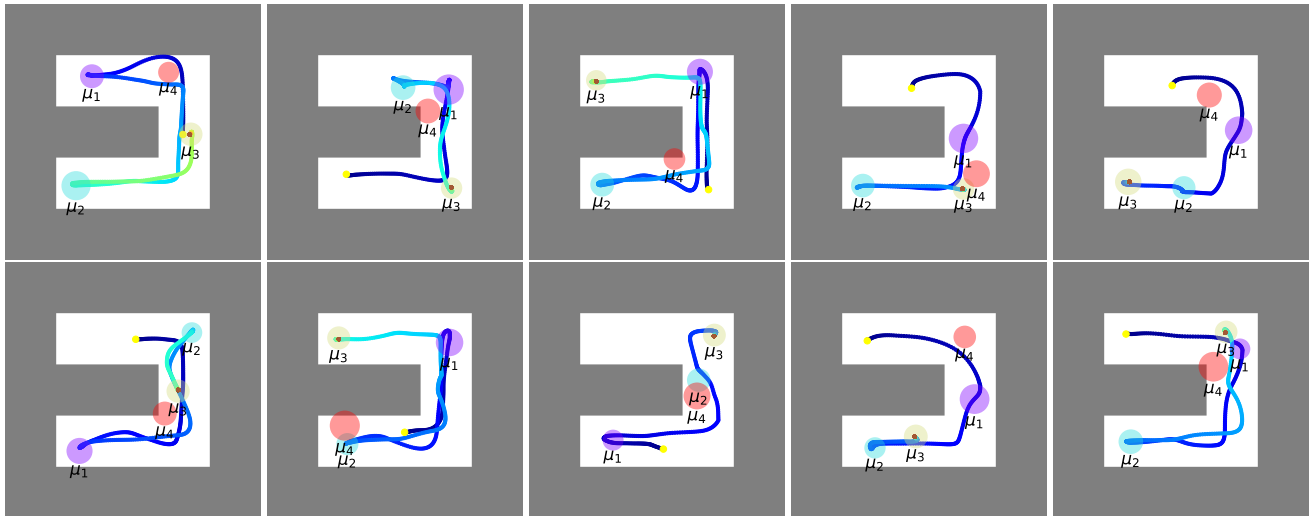


Figure E.3: Successful Execution Trajectories in Maze2D-umaze Environment under STL Template 5: $F_{I_1}(\mu_1 \wedge (F_{I_2}(\mu_2 \wedge F_{I_3}(\mu_3)))) \wedge G(\neg\mu_4)$. The task requires the agent to sequentially visit regions μ_1, μ_2, μ_3 within the given time intervals and always avoid the region μ_4 .

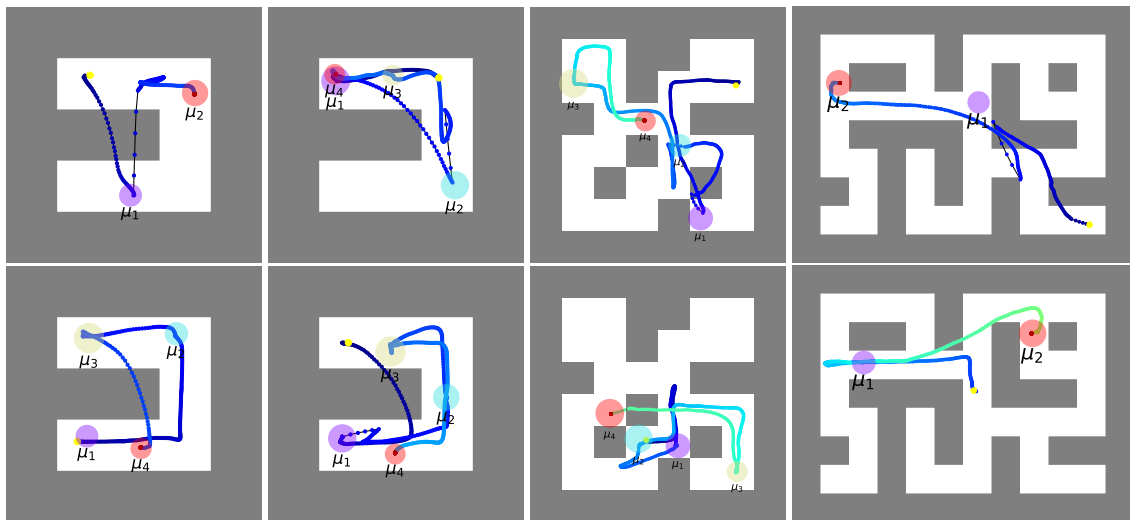


Figure E.4: Planned Trajectories in Some Failure Cases.